

A Theoretical Study of the Bifurcation Reaction II: Acetic Acid

Osamu TAKAHASHI, Kuniharu ITOH and Ko SAITO*

Department of Chemistry, Graduate School of Science, Hiroshima University,
1-3-1, Kagamiyama, Higashi-Hiroshima 739-8526, JPN

Abstract

The competing reactions in the thermal unimolecular decomposition of acetic acid were examined theoretically. Calculations of the transition state structures, the activation energies, and the intrinsic reaction coordinates (IRC) for the two competing reaction paths were performed by using the molecular orbital and the density functional theory. The potential barrier heights were mostly the same for the two competing reaction paths, which were consistent with previous studies. An examination of the mode coupling between the IRC and vibrational modes predicted no significant difference in the rates for the corresponding paths in agreement with experimental results. This is different from the case of formic acid which was reported in our previous paper of this series. The unimolecular reaction rate seems to be controlled by the number of effective vibrational modes which couple strongly with the IRC before the reactant arrives at the transition state.

1 Introduction

In our knowledge, most of the thermal unimolecular reaction occurs simultaneously with a few competitive reactions [?, ?, ?, ?, ?, ?, ?, ?, ?]. However, it is hard to deter-

mine the rate constant of each reaction path separately because of the complication due to consecutive reactions. Nevertheless, the investigation of the branching for these reaction paths is important not only for the reaction control in the industrial chemical systems but also for the kineticists to clear the dynamic behavior of each reaction path. The thermal decomposition of formic acid is known to occur with two reaction paths, i.e., dehydration and decarboxylation. In our previous shock tube study of the decomposition, Saito et al. found that the rates of these two competing paths differed substantially by about 30 times [?]. While, recent theoretical calculations gave similar potential barriers and also estimate nearly equal rate constants [?, ?, ?, ?, ?, ?, ?, ?]. This discrepancy between our experiment and these theoretical calculations seems to be attributed to calculation methods of the rate constant. Although the utility of the transition state theory and the RRKM theory is convenient to obtain the rate constant easily, the dynamic behavior along the reaction coordinate is not considered in these calculations. Recently, in the first paper of the series, we have discussed the relationship between the reaction rate and the curvature of the reaction path in the case of formic acid [?]. In this paper, it was found that in the dehydration path only one vibrational mode couples strongly with the intrinsic reaction coordinate (IRC) [?] in the course of the reaction, while in the decarboxylation path three modes mainly participate in the reaction. That is, the number of the effective mode which gives and takes the energy with the direction along the IRC is only one in the dehydration while the effective modes are three in the decarboxylation. In the present study, we try to confirm our proposal in the case of acetic acid.

There have been reported experimental [?, ?, ?, ?, ?, ?, ?] and theoretical [?, ?, ?, ?, ?, ?] investigations on the thermal decomposition of acetic acid in the gas phase. It is known that acetic acid has competing paths as follows,





where, reaction (3) of two-step mechanism was proposed in a theoretical research [?]. A shock tube study suggested the products of reaction (1) and (2) was produced in approximately equal amounts [?]. As a result, identical activation energies and pre-exponential factors were assigned for two reactions. Saito et al. [?] studied the thermal decomposition of acetic acid which was produced from shock heated ethyl acetate at high temperatures. They estimated the product ratio $[\text{CO}_2]/[\text{H}_2\text{O}]$ was around unity under their experimental conditions. With a pulsed CO_2 laser infrared multiphoton dissociation (IRMPD) in a collision less condition, Longfellow and Lee [?] confirmed that the branching ratio $[\text{CO}_2]/\{[\text{H}_2\text{O}] + [\text{CO}_2]\}$ was 0.54.

Theoretical studies for the decomposition of acetic acid have been reported by many groups [?, ?, ?, ?, ?, ?]. Sophisticated *ab initio* molecular orbital (MO) calculations were performed by Nguyen et al. [?], Duan and Page [?], and more recently, Moreira [?]. The most reliable energy barriers by Moreira are 75.4 for path (1), 71.5 for path (2), and 73.1 for path (3) in kcal mol^{-1} , where the value for path (3) corresponds to the TS of the first step. Under these backgrounds, we examined the reaction rate data obtained from experiments and theoretical calculations for the decomposition of acetic acid.

Potential energy barrier of reaction is one of the most important information for reaction dynamics, because it is reflected in the rate constant through the transition state theory. In addition, sequential information in the course of the reaction reflects the reaction dynamics directly. Therefore, detailed information of the potential energy surface is needed to discuss the reaction dynamics. Since, in experiment, it is very difficult to observe the molecular dynamics such as the reactant behavior and the energy distribution, we have to depend heavily on the theoretical calculation. It is popular to calculate the intrinsic reaction coordinate (IRC) [?] for the understanding of the reaction path which is defined as the steepest descent path in mass-weighted Cartesian coordinates. Detailed information of potential surface

is available from the vibrational analysis around the IRC's using the reaction path Hamiltonian approach by Miller et al. [?]

Recently, trajectory calculations have been performed routinely using semi-empirical MO [?] and *ab initio* MO [?] potentials. Although these methods do not include the quantum effect such as the tunneling effect, it is useful to examine the dynamics of reaction products. Generally, *ab initio* MO method is more accurate compared with the semi-empirical MO method, but the number of trajectories is limited because of lack of computer resources. Furthermore, to express precise process of the reaction, a multi-reference procedure such as the multi-configurational self-consistent field method and the multi-reference perturbation method should be required because the whole potential surfaces cannot be expressed precisely by a single reference theory such as the Hartree-Fock or the density functional theory (DFT). In the near future, dynamical calculations will be enable for relatively large molecules using the multi-reference theory.

In this paper, we treat the reaction of acetic acid in which the degree of freedom of the vibrational mode is larger than that of formic acid. In the previous paper [?], we treat the reaction of formic acid to solve the problem that one of the competing paths has abnormally large rate constant although the potential energy height is mostly the same with the other path. We think that it is very important to resolve this problem, because it constructs the concept of the chemical reaction rate.

2 Methods of Calculation

Ab initio MO and the DFT calculations are carried out with the GAUSSIAN98 [?] program package. All geometries of the reactants, products, and transition states (TSs) are determined with analytically calculated energy gradients at the DFT using Becke's three-parameter non-local exchange functional [?, ?, ?] and the non-local correlation functional of Lee, Yang and Parr [?](B3LYP) with Dunning's correlation consistent basis sets known as cc-pVDZ and cc-pVTZ [?]. Vibrational frequencies

are calculated by using the analytical second derivatives at the B3LYP/cc-pVDZ and B3LYP/cc-pVTZ to confirm the stationary structures and correct for the zero-point vibrational energy. Frequencies are scaled to 0.9613 times for the B3LYP calculations [?]. Although this value was determined for the 6-31G(d) basis set, not for the cc-pVDZ or cc-pVTZ basis sets, this treatment is thought to be a proper approximation. We verified that there is only one imaginary frequency for each TS.

The IRC calculations by Fukui [?] are followed from the TS toward both reactants and products. The normal vibrational analysis along the IRC was carried out by diagonalizing the Hessian matrices in the mass weighted coordinates after projecting out the component in the direction of the IRC. The reaction path Hamiltonian for a non-rotating polyatomic molecule, formulated by Miller et al. [?, ?], is used,

$$\begin{aligned}
 H(p_s, s, \{P_k, Q_k\}, k = 1, \dots, F - 1) \\
 = \frac{\frac{1}{2}[p_s - \sum_{k,k'}^{F-1} Q_k P_{k'} B_{k,k'}(s)]^2}{[1 + \sum_{k=1}^{F-1} Q_k B_{k,F}(s)]^2} + \frac{1}{2} \sum_{k=1}^{F-1} (P_k^2 + \omega_k(s)^2 Q_k^2) + V_0(s), \quad (4)
 \end{aligned}$$

where s and p_s are the reaction coordinate (IRC, in this case) and its conjugate momentum, respectively, $V_0(s)$ is the potential energy along the IRC as a function of s , and Q_k and P_k are coordinates and momenta for vibrations perpendicular to the IRC, with frequencies $\omega_k(s)$. The curvature coupling element $B_{k,F}$ mixes the vibrational mode k with the reaction coordinate s , and the intermode Coriolis coupling element $B_{k,k'}$ mixes the vibrational mode k and k' . These are defined as

$$B_{k,l}(s) = \frac{dL_k(s)}{ds} \cdot L_l(s), \quad (5)$$

where $L_k(s)$ ($k = 1, \dots, F - 1$) and $L_F(s)$ denote the k th normal mode vector and the normalized gradient vector, respectively. Here, all the force constants and coupling elements are truncated at the second order. The total curvature of the IRC $\kappa(s)$ is the magnitude of the $(F - 1)$ dimensional vector made of $B_{k,F}$:

$$\kappa(s) = \left[\sum_{k=1}^{F-1} B_{k,F}(s)^2 \right]^{1/2}. \quad (6)$$

3 Results and Discussions

3.1 Rate constants and kinetics

Fig. 1 shows the schematic energy profile with zero-point energy corrections and optimized geometries for cis-, trans-acetic acid, TSs for path (1), (2) and (3). And Table 1 shows relative energies using various calculation levels of theory. These geometries are quite similar to the previous results of *ab initio* calculations [?, ?, ?]. Calculated vibrational frequencies at the B3LYP/cc-pVTZ level are given in Table 2.

Using these results, rate constants for path (1), (2) and (3) are estimated from the conventional transition state theory in the temperature range of 1300 - 2000 K, which is covered with the experimental conditions by Saito et al [?]. Pre-exponential factor A (in s^{-1}) and activation energy E_a (in kcal mol^{-1}) for each reaction path are listed in Table 3. In Fig. 2, Arrhenius plots are shown for our calculations using the conventional transition state theory and for experiments. In our calculations, rate constants for three reaction paths are mostly comparable, i.e., the difference between k_1 and k_2 is within a factor of three or four, and these results are consistent with Duan and Page [?].

3.2 The IRC calculations

To get much information for the potential energy surface of the reaction path, the IRC calculations are performed for each path. In the following discussion, we limit our attention to paths (1) and (2). For a two-step reaction path (3), since energy redistribution between vibrational modes will occur in an intermediate compound, it is difficult to discuss the dynamics of the reaction from the reactant to the product along the IRC. Vibrational frequencies along the IRC for the two paths are shown in Fig. 3 (a) and (b). And the corresponding behavior of couplings with the IRC are shown in Fig. 4 (a) and (b). The horizontal line means the mass-weighted reaction

coordinate in both figures and zero corresponds to the TS. Positive and negative sides correspond to the product and the reactant from the TS, respectively. In the case of path (1), there are a few vibrational modes that relate directly with the reaction, for example, the CH stretching. In this reaction path, one of hydrogen atoms in the CH₃ group transfer to the OH group, then produce CH₂CO and H₂O. This behavior reflects in the curvature of the IRC. As seen in Fig. 4(a), only one large peak arises at around $s = 0.5$. By examining the vibrational character, it is found that the mode to contribute mainly at this peak is the CH stretching. That is, the energy transfer between the CH stretching and the IRC becomes larger at this region. It is noted that some vibrational modes such as the CH stretching and the HCH twisting contribute to the curvature in the range of negative s . A similar discussion is done for path (2). As seen in Fig. 3(b), there are a few vibrational modes that couple to the IRC strongly. These are the CO and the OH stretching modes. For the corresponding curvature, Fig. 4(b), one large peak arises at around $s = 0.5$, the same position as path (1) accidentally. The main components to contribute to this peak are the CO and the OH stretching modes respectively. Additionally, some vibrational modes such as the OH stretching and the CH₃ rocking are contributed to the curvature in the range of the negative s . Here, if we discuss the decomposition rate, it is important to consider the negative s region, since the reaction rate depends on the time to take from the initial reactant state to the TS. The positive s region rather corresponds to the product information.

Since there is the kinetic energy for each vibrational mode in the reacting molecule, the real reaction paths deviate from the IRC. Nevertheless, the importance of the behavior around the IRC was pointed out by Michalak and Ziegler, [?] using the *ab initio* molecular dynamics simulations. From our present calculations, not only the potential barrier heights are similar in the two paths but also the behavior around the IRC are not different from each other. Furthermore, before the reactions arrive at the TS, some vibrational modes strongly couple to the IRC, indicating that the energy transfer happens between the IRC and these vibrational modes. In the previ-

ous paper, [?] we have discussed the relation between the amount of energy transfer between vibrational modes (or the number of the couplings) and the reaction rate. From our theoretical studies it seems that both reaction paths for the acetic acid decomposition proceed statistically on the contrary to formic acid. That is, in the case of acetic acid, the experimental results may be explained reasonably by the statistical theories, and it is difficult to distinguish the rates between the two paths. This is consistent with the experimental results.

3.3 Difference of reactivity between formic and acetic acid

In this section, we discuss the difference in the competing reactions between formic and acetic acid. These are fatty acids including one and two carbon atoms, and both have similar competing decomposition paths in the gas phase. In the case of formic acid, the following mechanism is given, i.e., dehydration (7) and decarboxylation (8).



It is noted that path (7) proceeds through the three-center TS, on the other hand, path (8) proceeds through the four-center TS. As briefly mentioned in Introduction, Saito et al. [?] have reported that, contrary to the results of Hsu et al. [?] performed under the some conditions of the shock tube method, the rates of these two competing paths differed each other by a factor of 30 [?], being consistent with the other experiments [?, ?, ?]. Potential energy barriers of these paths evaluated from high-level MO calculations are comparable [?, ?, ?, ?, ?]. Therefore, at a first glance, the rate constants are expected to be the same order for the two paths, contrary to the experiment. In fact, theoretical calculations using the statistical method (the transition state theory) gave similar rate constants [?]. On the other hand, for acetic acid the competing paths proceed through four-center TSs. It has been confirmed by previous experiments that the rate constants of path (1) and (2) are nearly equal.

Also, theoretically, previous investigations and present calculations give comparable energy barrier heights for these paths resulting the similar rate constants.

According to the classical RRK theory, the high pressure rate constant is given as follows,

$$k(E) = \nu \left(\frac{E - E_0}{E} \right)^{s-1} \quad (9)$$

where, ν is the vibrational frequency for the critical oscillator, E and E_0 are the total and critical energy, and s is the number of classical oscillators. From Eq. (9), one can find that the larger the number of s becomes, the smaller rate constant becomes. However, the concept of “classical oscillator” is not clear in the RRK theory. In general, the number of classical oscillators is interpreted as the number of effective vibrational mode which contributes to the reaction. These correspond to vibrational modes contributing the curvature of the IRC. In the case of acetic acid, the number of vibrational modes contributing to the curvature is similar whereas, this number differs in the case of formic acid, i.e., that for the path (7) is less than that for the path (8) at high pressures. This implies that the rate of reaction (7) is larger than that of reaction (8). In order to evaluate the rate quantitatively, we need more detailed information for reaction paths of these molecules.

To discuss the reactivity of the unimolecular reaction, various information about the process from the reactant to the transition state is important, not just only the TS. In the case of acetic acid, many vibrational modes contribute to paths (1) and (2) until the reactant reaches to the TS. On the other hand, in the case of formic acid, the characteristics are different between paths (7) and (8). The number of vibrational modes that couple to the IRC for path (7) is abnormally less compared to path (8). Furthermore, the magnitude of the couplings between vibrational modes in the reactant through path (7) is also smaller compared to path (8). In other words, the energy transfer between vibrational modes is constrained in path (7). These phenomena suggest that it is difficult to exchange the energy of vibrational modes with the IRC mode smoothly. The slow exchange of intramolecular vibrational energy redistribution between active and inactive vibrational states is known as

'non-RRKM behavior' [?]. In the case of path (7), the behavior is likely to this.

From above discussions, reasons for the difference of the reactivity between formic and acetic acid are appeared. First, the difference of the number of the degree of freedom differs in these molecules, i.e., nine for formic acid and eighteen for acetic acid. The RRKM behavior is expected for the molecules which have large number of degree of freedom, for example, more than ten. Second, the character of the intramolecular energy transfer of each path to the TS, couplings with the IRC and couplings between vibrational modes is different in the two acids. It seems that the difference of the reactivity for the competing paths arises for small molecules which have the vibrational freedoms around ten.

4 Summary

In this paper, we have studied the unimolecular decomposition of acetic acid using the MO and DFT theory, and examined the character around the IRC in detail using the reaction path Hamiltonian by Miller et al. The reactivity of the two competitive channels have been discussed semi-quantitatively. Difference for two competing paths, dehydration (1) and decarboxylation (2), was not observed by the conventional transition state theory using high-level MO and DFT calculations, because both energy barriers of reaction and the couplings of each vibrational mode with the IRC are not different in the two paths. These are in agreement with previous experimental and theoretical results.

It was found that difference of the reactivity between formic and acetic acid was originated not only the number of degree of freedom in the molecule but also from the amount of coupling between the IRC and vibrational modes. It is seemed that dehydration of formic acid is the special case, i.e., a kind of intrinsic non-RRKM behaviors.

5 Acknowledgement

This study is supported by a Grant-in-Aid on Research for the Future “Photoscience” (JSPS-RFTF-98P01202) from Japan Society for the Promotion of Science. The authors thank the Institute for Numerical Simulations and Applied Mathematics at Hiroshima University, for the use of COMPAQ Personal Workstation 433au.

Table 1: Relative energies(in kcal mol⁻¹) from zero point energy level of cis-CH₃COOH. Zero point energy correction is added for each case.

	cis- CH ₃ COOH	trans- CH ₃ COOH	TS1 ^a	CH ₂ CO+H ₂ O	TS2 ^a	CH ₄ +CO ₂
B3LYP/cc-pVDZ	0.0	5.7	70.0	36.9	66.8	-12.6
B3LYP/cc-pVTZ	0.0	5.2	70.4	30.5	67.6	-0.1
MP4/cc-pVDZ// B3LYP/cc-pVDZ	0.0	5.2	70.9	32.5	66.9	-14.3
MP4/cc-pVTZ// B3LYP/cc-pVTZ	0.0	5.2	71.0	32.8	67.0	-13.7
	TS3-1 ^a	CH ₂ =C(OH) ₂	TS3-2 ^a			
B3LYP/cc-pVDZ	68.8	28.4	69.2			
B3LYP/cc-pVTZ	70.0	27.0	68.7			
MP4/cc-pVDZ// B3LYP/cc-pVDZ	71.1	28.6	70.0			
MP4/cc-pVTZ// B3LYP/cc-pVTZ	71.0	28.6	70.1			

^a TS1 and TS2 mean transition state for path (1) and (2). TS3-1 and TS3-2 mean the first and the second transition state for path (3).

Table 2: Unscaled vibrational frequencies(in cm^{-1}) using B3LYP/cc-pVTZ level of theory.

compound	vibrational frequencies
cis-CH ₃ COOH	77.7 ,423.1 ,547.0 ,585.2 ,670.6 ,859.3 ,998.8 ,1070.3 ,1204.8 ,1341.8 , 1408.9 ,1473.3 ,1478.6 ,1825.9 ,3052.6 ,3109.2 ,3160.6 ,3743.8
trans-CH ₃ COOH	109.2 ,431.4 ,473.5 ,598.3 ,599.1 ,856.0 ,988.0 ,1064.5 ,1205.5 ,1297.8 , 1395.8 ,1474.2 ,1488.0 ,1860.7 ,3036.0 ,3091.5,3154.4 ,3801.8
TS1	1810.5i,283.3 ,426.2 ,466.2 ,540.0 ,630.6 ,707.8 ,819.2 ,858.4 ,1048.5 , 1102.0 ,1341.4 ,1455.2 ,1819.7 ,2051.9 ,3117.7,3200.0 ,3790.0
TS2	2032.5i,221.6 ,326.2 ,493.8 ,580.4 ,619.0 ,727.8 ,781.1 ,1125.4 ,1216.2 , 1309.6 ,1424.7 ,1442.8 ,1791.4 ,2079.9 ,2952.2,3119.0 ,3188.1
TS3	2082.3i,426.6 ,495.1 ,558.6 ,621.3 ,738.8 ,806.8 ,996.4 ,1067.2 ,1135.2, 1208.4 ,1415.8 ,1505.1 ,1587.0 ,1952.0 ,3113.0,3194.6 ,3740.9
TS4	1668.3i, 391.1, 443.1, 573.4, 599.7, 628.7, 719.2, 987.5, 1013.4, 1180.0, 1326.2, 1441.1, 1825.1, 2107.8, 3185.7, 3283.5, 3753.1
CH ₂ CO	442.7 ,552.4 ,593.7 ,990.6 ,1171.9 ,1413.1 ,2222.3 ,3181.1 ,3273.0
H ₂ O	1639.3 ,3800.9 ,3901.3
CH ₄	1282.1 ,1282.1 ,1282.1 ,1521.4 ,1521.4 ,3131.0 ,3260.6 ,3260.6 ,3260.6
CO ₂	671.9 ,671.9 ,1371.6 ,2416.6
CH ₂ =C(OH) ₂	185.0 ,373.1 ,456.9 ,532.8 ,655.2 ,688.8 ,742.0 ,934.7 ,978.9 ,1181.4, 1234.1 ,1407.5 ,1447.4 ,1755.8 ,3179.2 ,3272.5,3807.7 ,3826.3

Table 3: Arrhenius parameters for the decomposition of acetic acid using the conventional transition state theory in temperature range of 1300 - 2000 K, and rate constants at 1600 K.

path (1)			
	A / s ⁻¹	E _a / kcal mol ⁻¹	k / s ⁻¹
MP4/cc-pVTZ//B3LYP/cc-pVDZ	4.24 × 10 ¹³	73.7	3.64 × 10 ³
MP4/cc-pVTZ//B3LYP/cc-pVTZ	5.46 × 10 ¹³	73.9	4.40 × 10 ³
path (2)			
	A / s ⁻¹	E _a / kcal mol ⁻¹	k / s ⁻¹
MP4/cc-pVTZ//B3LYP/cc-pVDZ	5.26 × 10 ¹³	69.6	1.64 × 10 ⁴
MP4/cc-pVTZ//B3LYP/cc-pVTZ	5.25 × 10 ¹³	69.7	1.58 × 10 ⁴
path (3)-1			
	A / s ⁻¹	E _a / kcal mol ⁻¹	k / s ⁻¹
MP4/cc-pVTZ//B3LYP/cc-pVDZ	8.21 × 10 ¹²	72.9	9.05 × 10 ²
MP4/cc-pVTZ//B3LYP/cc-pVTZ	9.08 × 10 ¹²	72.8	1.03 × 10 ³

Figure captions.

- Fig.1 Relative energy profile of competing decomposition pathways for acetic acid with zero-point energy corrections. MP4/cc-pVTZ//B3LYP/cc-pVTZ level of theory.
- Fig.2 Comparison of rate constants. Solid and dashed lines indicate calculated and experimental rate constants, respectively. Calculated rate constants are obtained using the conventional transition state theory in temperature range of 1300 - 2000 K.
- Fig.3 Vibrational frequencies for the decomposition of acetic acid along the IRC using B3LYP/cc-pVTZ level of theory. (a)path (1) and (b)path (2).
- Fig.4 The IRC curvatures κ and coupling $|B|$ with the IRC for the decomposition of acetic acid along the IRC using B3LYP/cc-pVTZ level of theory. (a)path (1). (b)path (2). For both Figs., a thick solid line indicates curvature $\kappa(s)$.

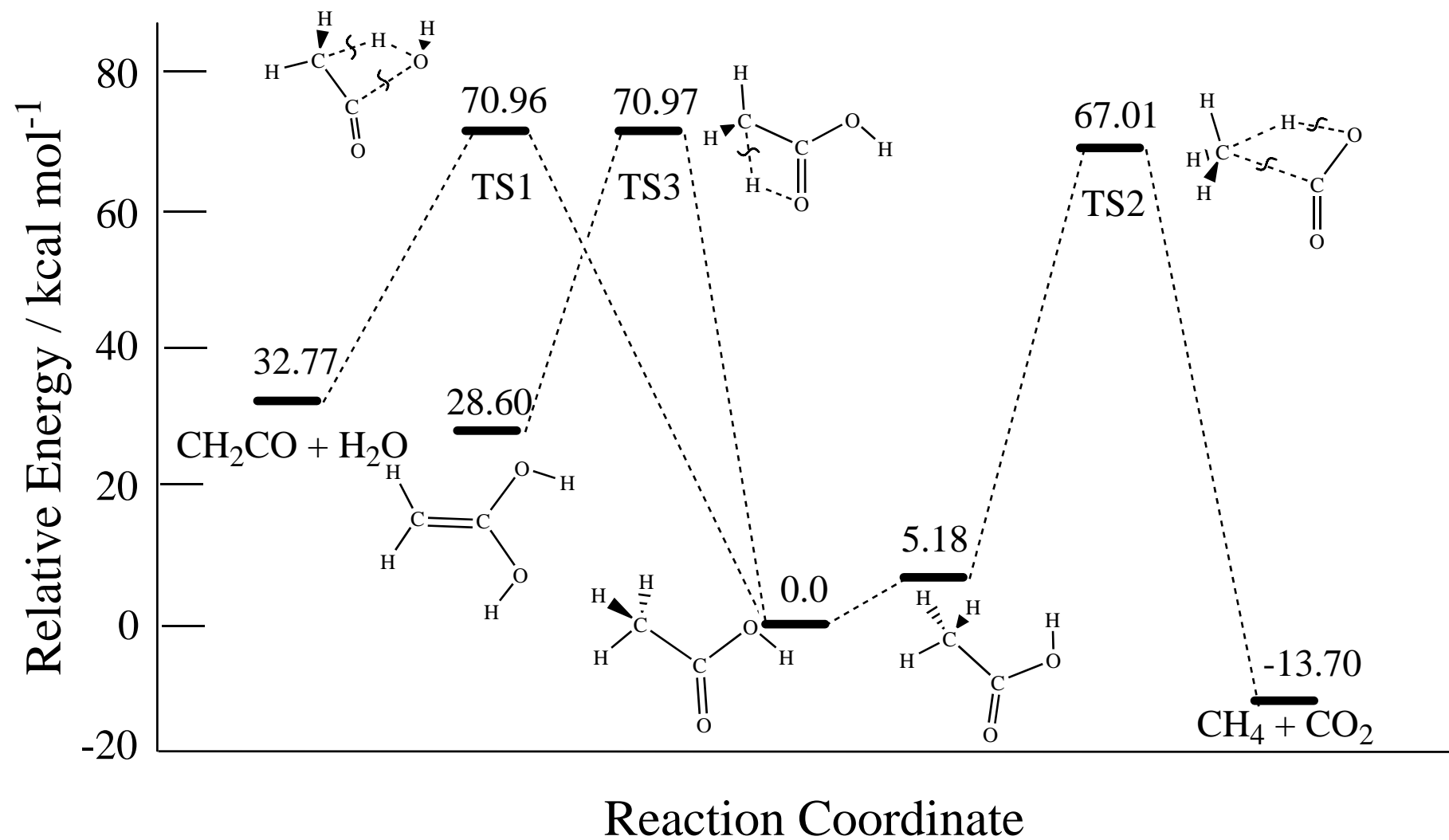


Fig.1 Takahashi et al.

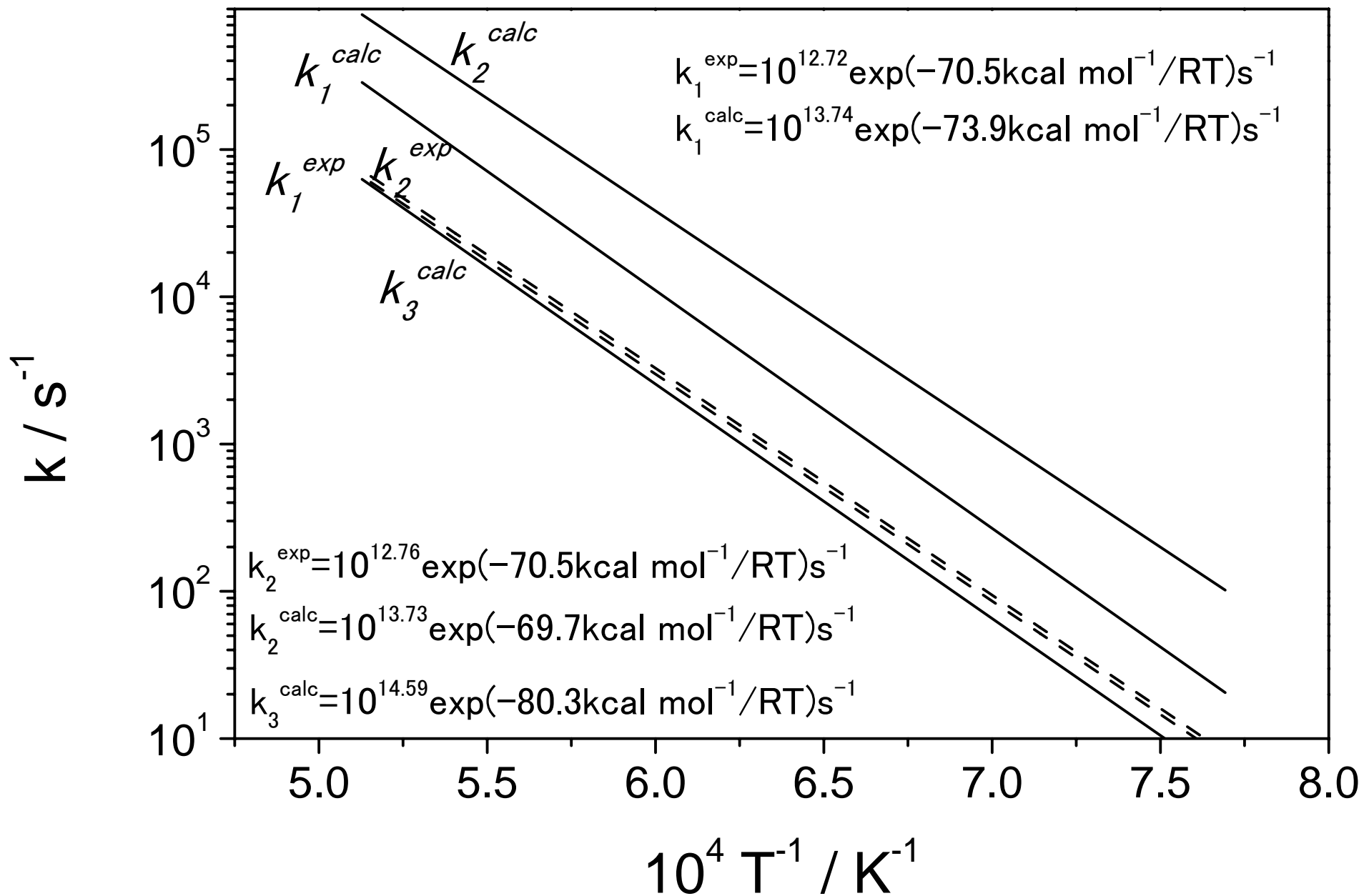


Fig. 2 Takahashi et al

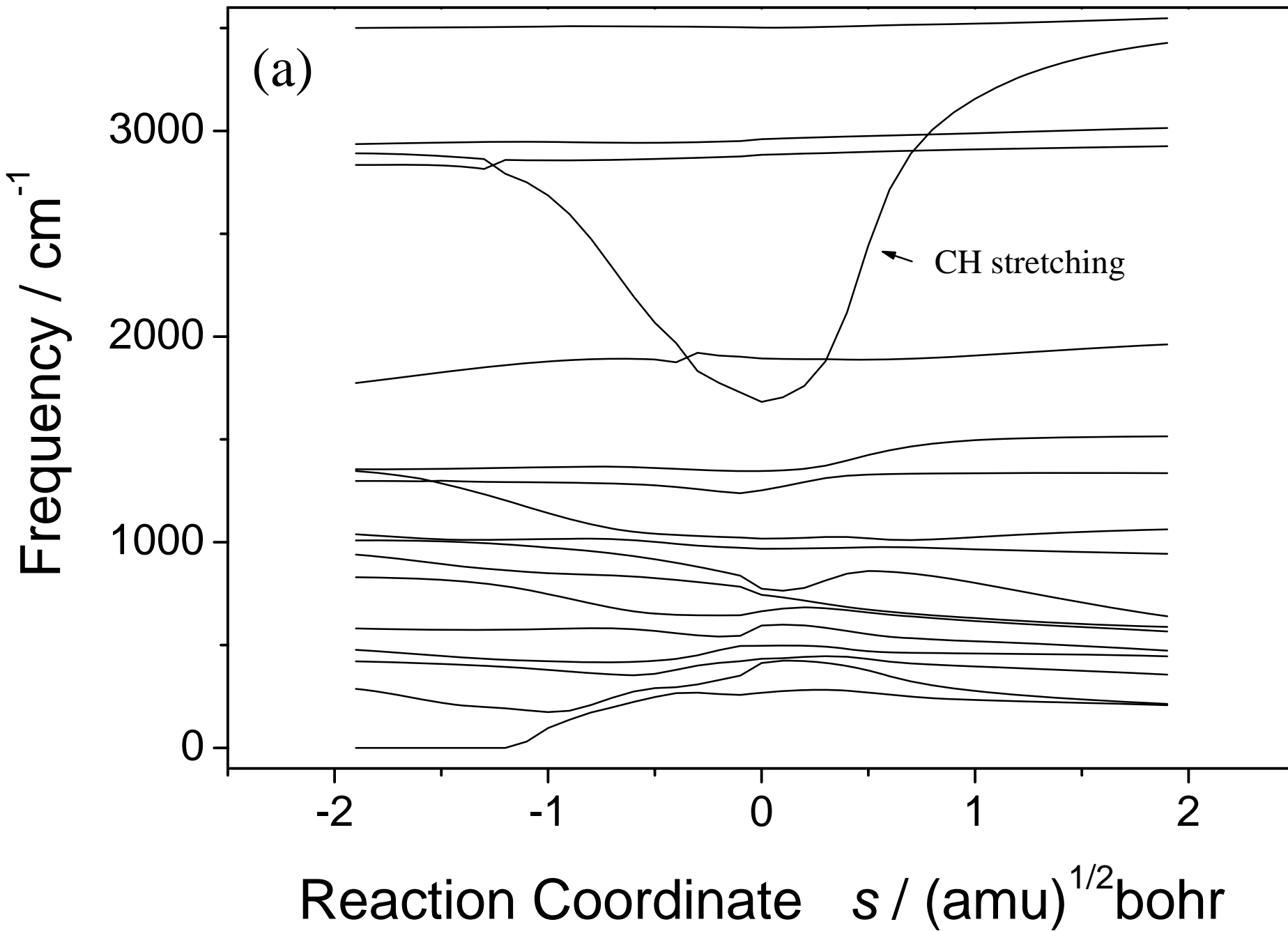


Fig.3(a) Takahashi et al.

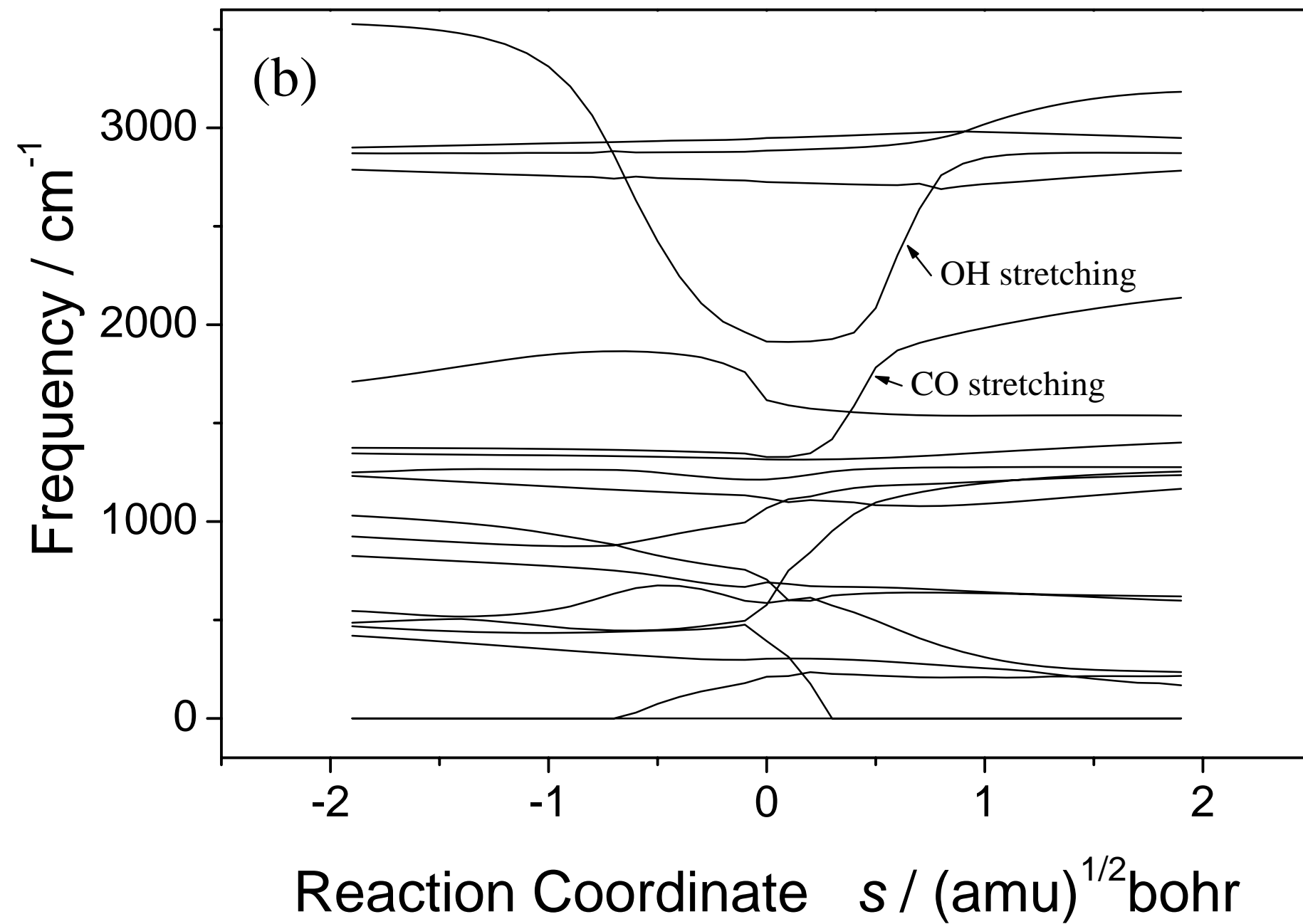


Fig.3(b) Takahashi et al.

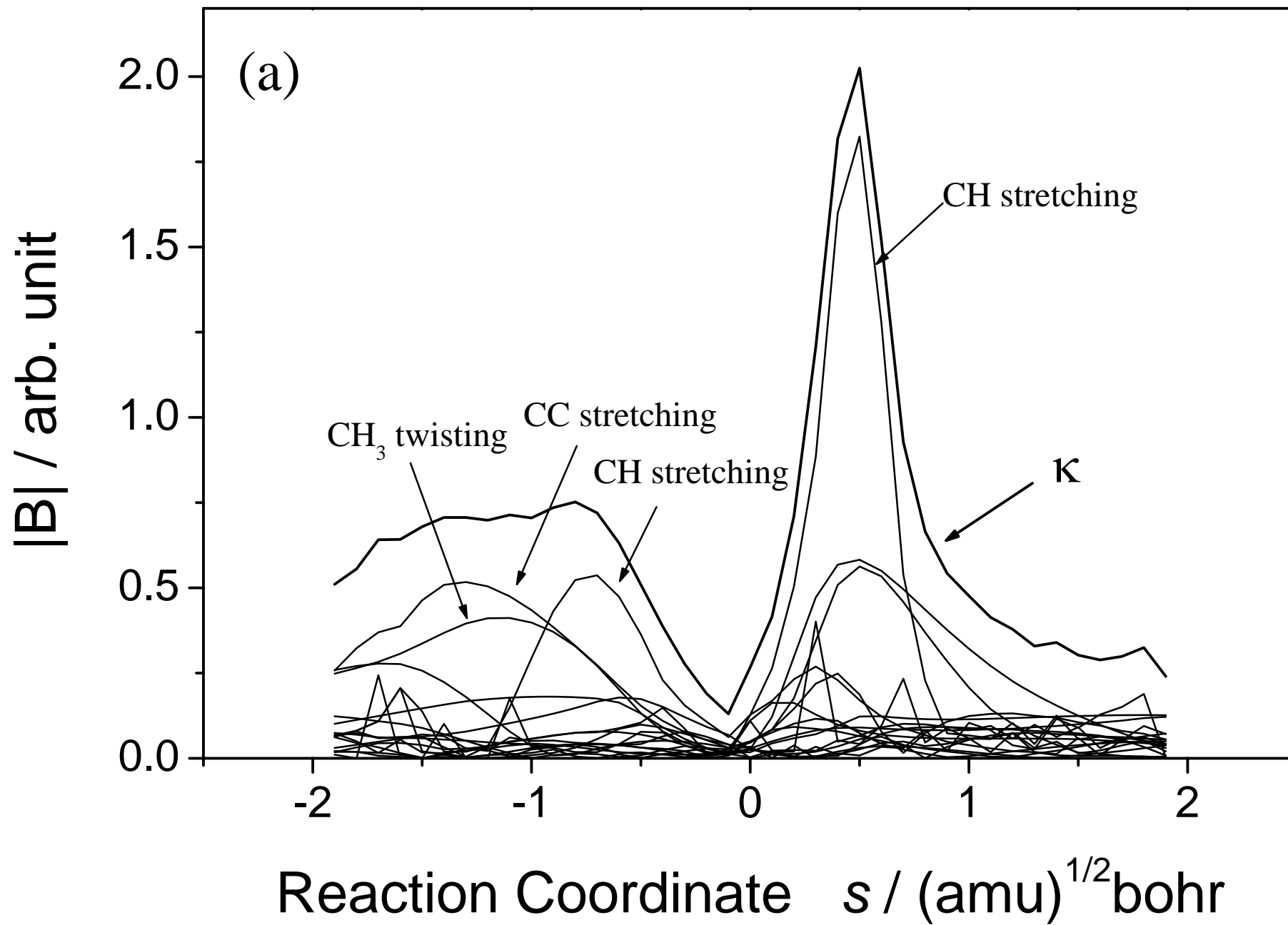


Fig.4(a) Takahashi et al.

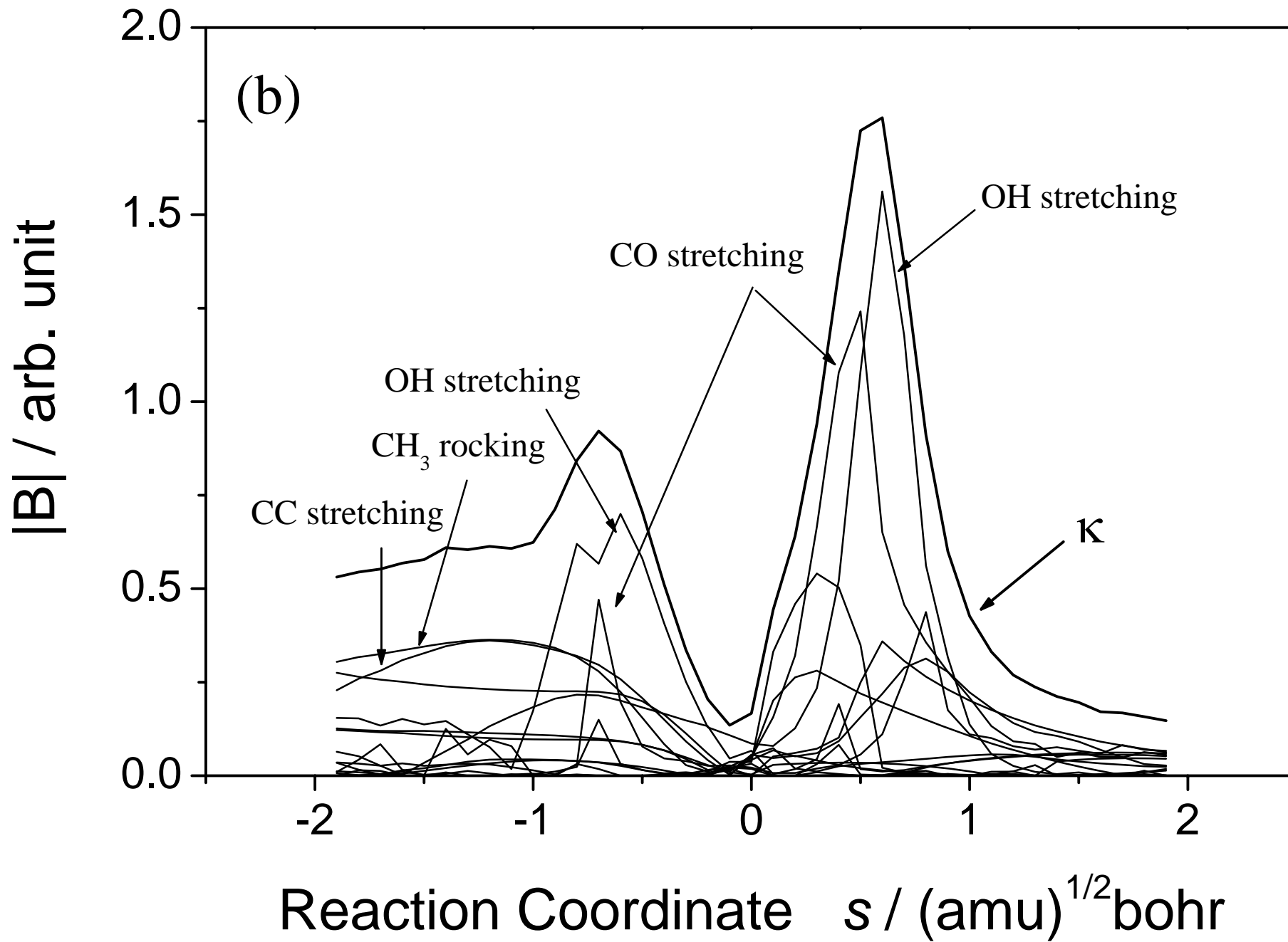


Fig.4(b) Takahashi et al.